UC Davis
UC Davis Previously Published Works

Title

Drawn-on-Skin Sensors from Fully Biocompatible Inks toward High-Quality Electrophysiology (Small 36/2022)

Permalink

Journal

Small, 18(36)

ISSN

Authors

Patel, Shubham
Ershad, Faheem
Lee, Jimmy
et al.

Publication Date

2022-09-01

DOI

Peer reviewed

Drawn-on-Skin Sensors from Fully Biocompatible Inks toward High-Quality Electrophysiology

Shubham Patel, Faheem Ershad, Jimmy Lee, Lourdes Chacon-Alberty, Yifan Wang, Marco A. Morales-Garza, Arturo Haces-Garcia, Seonmin Jang, Lei Gonzalez, Luis Contreras, Aman Agarwal, Zhoulyu Rao, Grace Liu, Igor R. Efimov, Yu Shrike Zhang, Min Zhao, Roslyn Rivkah Isseroff, Alamgir Karim, Abdelmotagaly Elgalad, Weihang Zhu, Xiaoyang Wu, and Cunjiang Yu*

The need to develop wearable devices for personal health monitoring, diagnostics, and therapy has inspired the production of innovative on-demand, customizable technologies. Several of these technologies enable printing of raw electronic materials directly onto biological organs and tissues. However, few of them have been thoroughly investigated for biocompatibility of the raw materials on the cellular, tissue, and organ levels or with different cell types. In addition, highly accurate multiday in vivo monitoring using such on-demand, in situ fabricated devices has yet to be done. Presented herein is the first fully biocompatible, on-skin fabricated electronics for multiple cell types and tissues that can capture electrophysiological signals with high fidelity. While also demonstrating improved mechanical and electrical properties, the drawn-on-skin ink retains its properties under various writing conditions, which minimizes the variation in electrical performance. Furthermore, the drawn-on-skin ink shows excellent biocompatibility with cardiomyocytes, neurons, mice skin tissue, and human skin. The high signal-to-noise ratios of the electrophysiological signals recorded with the DoS sensor over multiple days demonstrate its potential for personalized, long-term, and accurate electrophysiological health monitoring.

1. Introduction

With the increasing demand for personalized wearable healthcare monitoring systems, wearable bioelectronic devices that are tailored to each individual are of considerable interest. Recent literature demonstrates a greater effort to develop mechanically and electrically stable materials and fabrication approaches that can be adapted for on-demand, rapid healthcare monitoring, and diagnostics.[1–3] Such materials and fabrication approaches allow for the capture of a multitude of vital physiological parameters including electrocardiogram (ECG), electromyogram (EMG), electroencephalogram (EEG), and electrooculogram (EOG) signals. In several cases of healthcare diagnostics, devices possessing specific designs are required to adequately match the shape and texture of the target surface. Knowing the minute design requirements beforehand to

S. Patel, W. Zhu, C. Yu
Department of Mechanical Engineering
University of Houston
Houston, TX 77204, USA
E-mail: cyu13@central.uh.edu
F. Ershad, Y. Wang, L. Gonzalez, L. Contreras, C. Yu
Department of Biomedical Engineering
University of Houston
Houston, TX 77204, USA
J. Lee, X. Wu
Ben May Department for Cancer Research
The University of Chicago
Chicago, IL 60637, USA
L. Chacon-Alberty
Regenerative Medicine Research
Texas Heart Institute
Houston, TX 77030, USA

M. A. Morales-Garza, A. Elgalad
Cardiovascular Surgery Research
Texas Heart Institute
Houston, TX 77030, USA
A. Haces-Garcia, C. Yu
Department of Electrical and Computer Engineering
University of Houston
Houston, TX 77204, USA
S. Jang, Z. Rao, C. Yu
Materials Science and Engineering Program
University of Houston
Houston, TX 77204, USA
A. Agarwal, A. Karim
Department of Chemical and Biomolecular Engineering
University of Houston
Houston, TX 77204, USA
G. Liu
Bellaire High School
Bellaire, TX 77041, USA

ADVANCED
SCIENCE NEWS
www.advancedsciencenews.com

NANO · MICRO
small
www.small-journal.com

prefabricate devices for such applications is thus challenging. Furthermore, the typical approach for wearable bioelectronics, which involves first fabricating the devices and then laminating them to the target surfaces, typically requires complex, costly, and/or high-temperature procedures. Techniques that allow users to design and fabricate inexpensive yet reliable devices for on-site applications directly onto the skin or other organs or tissues are extremely attractive in such scenarios.

Recent advances in materials and device fabrication techniques have led to electronic materials being deposited directly onto the skin for device fabrication. Metal nanoparticles/nanowires have been directly printed and/or sintered on human skin at room temperature to construct various body sensors to measure temperature, hydration, ECG, EMG and also for wireless functions.[4–8] A bioactive conductive pen has been developed to hand-draw blood glucose sensors directly on human skin.[9] Liquid metal inks have been paint-brushed or roller-coated onto target tissues for tumor-site therapy and vital sign monitoring. Still, nearly all the existing literature of on-site electronic device fabrication took little consideration of the biocompatibility of their materials on the cellular, tissue, and organ levels. Also, none of those studies demonstrated high-fidelity and multiday electrophysiological (EP) monitoring.

Here we present a highly conductive and fully biocompatible ink based on the drawn-on-skin (DoS) sensor platform[10] with which the inks can be directly deposited by a modified ballpoint pen onto the human skin. After drying, the ink produces a thin, stretchable film that conformally interfaces with the skin. The ink is in the form of a composite consisting of Ag flakes and poly(3,4-ethylenedioxythiophene): polystyrene sulfonate (PEDOT:PSS) modified with a triblock copolymer, poly(ethylene glycol)-block-poly(propylene glycol)-block-poly(ethylene glycol) (PEO_{20}-PPO_{70}-PEO_{20}, Pluronic P123). The mechanical, electrical, and writing properties of the DoS ink are characterized. We demonstrate the biocompatibility of the ink through cell viability and toxicity assays using rat neonatal cardiomyocytes (CMs) and cortical neurons. Histological and immunochemistry studies are performed on the skin of living mice to check for potential inflammatory markers over a few days of wearing
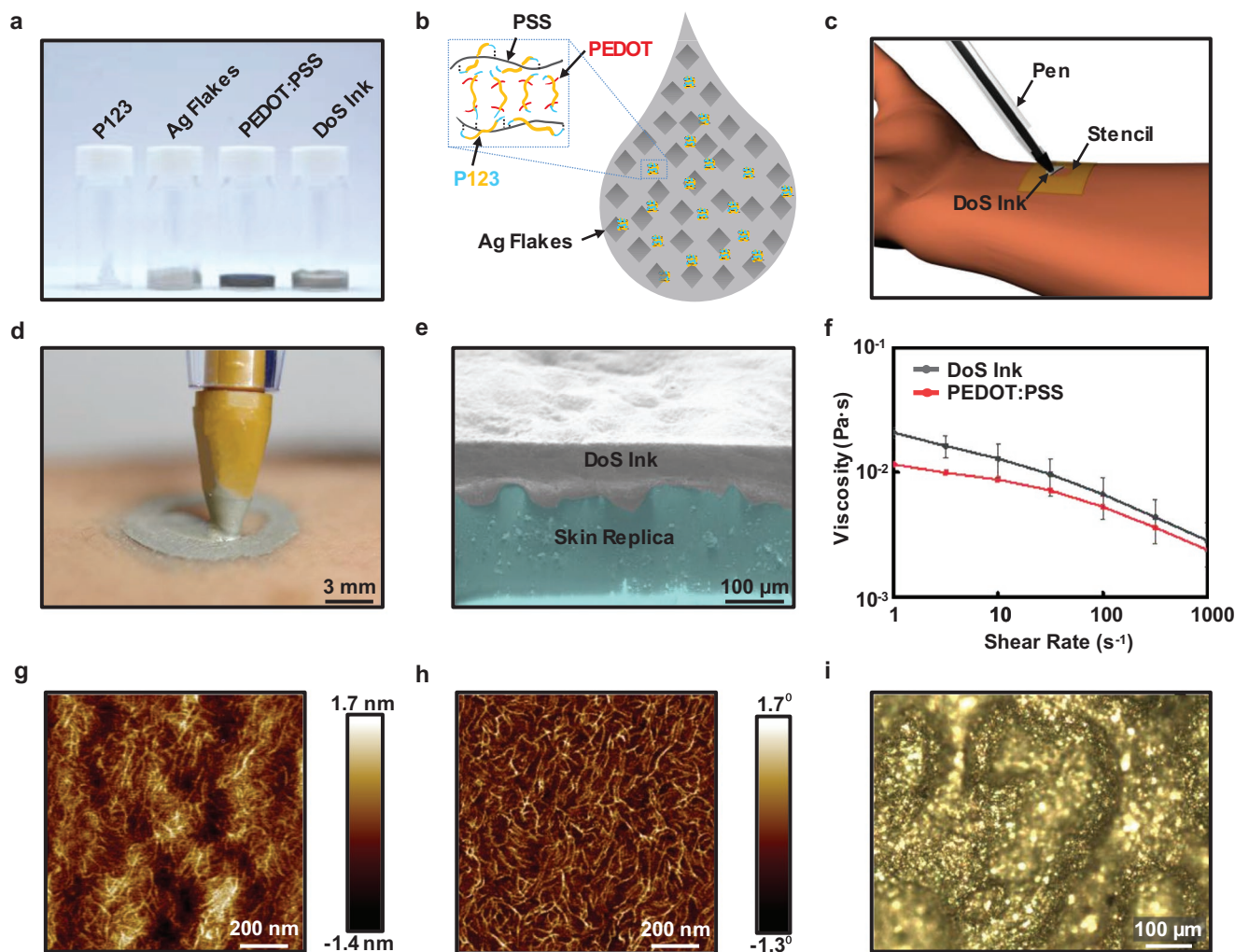
I. R. Efimov
Department of Biomedical Engineering
The George Washington University
Washington, DC 20052, USA

Y. S. Zhang
Division of Engineering in Medicine
Department of Medicine
Brigham and Women's Hospital
Harvard Medical School
Cambridge, MA 02139, USA

M. Zhao, R. R. Isseroff
Department of Dermatology
University of California Davis
Sacramento, CA 95816, USA

W. Zhu
Department of Engineering Technology
University of Houston
Houston, TX 77204, USA

C. Yu
Texas Center for Superconductivity
University of Houston
Houston, TX 77204, USA

the ink. Through the development of a novel connection scheme, critical EP signals, such as ECG, EMG, EEG, and EOG, are captured with high quality. In particular, the EEG signals are reliably recorded over multiple days. A human–machine interface (HMI) is implemented by employing the DoS EOG signals to control a virtual character in a video game. The development of such a biocompatible ink expands the library of DoS electronic materials and encourages deeper investigation into the materials–biology interactions, while holding promise in rapid, on-site, customizable, and personalized medical care.

2. Results and Discussion

2.1. DoS Ink Preparation and Material Characterizations

The DoS conductive ink was prepared by creating a composite of Ag flakes and P123-modified PEDOT:PSS solution (**Figure 1**a). Details of the ink preparation can be found in the Experimental Section. The schematic of the ink is shown in Figure 1b. PEDOT:PSS is an intrinsically conductive polymer consisting of PEDOT, a hydrophobic conductive conjugated polymer, and PSS, the hydrophilic nonconductive part of the polymer, having high mechanical flexibility and good biocompatibility.[11,12] However, introducing certain surfactants to PEDOT:PSS can enhance its electrical conductivity and mechanical stretchability. Here, we utilized P123, a triblock copolymer that weakens the ionic interaction between PEDOT and PSS due to the hydroxyl group of P123, which forms hydrogen bonds with PSS, thus helping in the aggregation of the PEDOT chains. Due to this plasticizing effect of P123 on PEDOT:PSS, an increased electrical conductivity and high mechanical stretchability of PEDOT:PSS can be achieved.[12] Adding Ag flakes to the P123-modified PEDOT:PSS could lead to significantly increased conductivity. Overall, the combination of the Ag flakes and P123-modified PEDOT:PSS forms a stretchable, highly conductive composite ink.

The required device was prepared by first making the stencil (based on Kapton tape) with a cutting machine (Silhouette Cameo), adhering the stencil to the target skin, and then drawing onto the outline of the stencil with the DoS ink using a modified ballpoint pen (Figure 1c,d). The DoS ink was drawn conformally onto the skin, as shown in Figure 1d. The scanning electron microscope (SEM) image of the cross-section of the interface of the DoS ink and polydimethylsiloxane (PDMS)-based skin replica (Figure 1e) proves the conformality of the DoS ink on the targeted substrate, as it can be seen clearly that the ink fills all crevices of the PDMS skin replica well. The skin replica was made using a porcine skin model. A rheological measurement was carried out at room temperature for the DoS ink and the P123-modified PEDOT:PSS (without Ag) ink. The shear rate-viscosity profiles for the DoS ink and the P123-modified PEDOT:PSS ink are shown in Figure 1f. The viscosity of the P123-modified PEDOT:PSS and DoS ink ranged from 0.116 to 0.023 Pa s and 0.207 to 0.028 Pa s, respectively, for shear rates from 1 to 1000 s^{-1}. This viscosity range is similar to that reported in other literature.[13–15] It should also be noted that the addition of P123 increases the viscosity of the ink so that it does not all flow all out of the pen during drawing. The power-law index (n)

Figure 1. a) From left to right, image of vials containing P123, Ag Flakes, PEDOT:PSS, and DoS ink respectively. b) Schematic of a possible molecular arrangement of DoS ink. c) Schematic of DoS ink device fabrication. d) Device being drawn with a modified ballpoint pen. e) SEM image of interface of the DoS ink and skin replica over which the ink has been drawn. f) Viscosity of DoS ink and P123-modified PEDOT:PSS ink at shear rates ranging from 1 to 1000 s^{-1} ($n = 4$). g) AFM topography and h) phase image of P123-modified PEDOT:PSS ink. i) Optical microscopic image of DoS ink drawn over skin replica.

was calculated by applying the power-law model[16] to the shear rate-viscosity profiles, so the fluid behavior of the ink could be ascertained. The power-law model equation[16,17] is given by
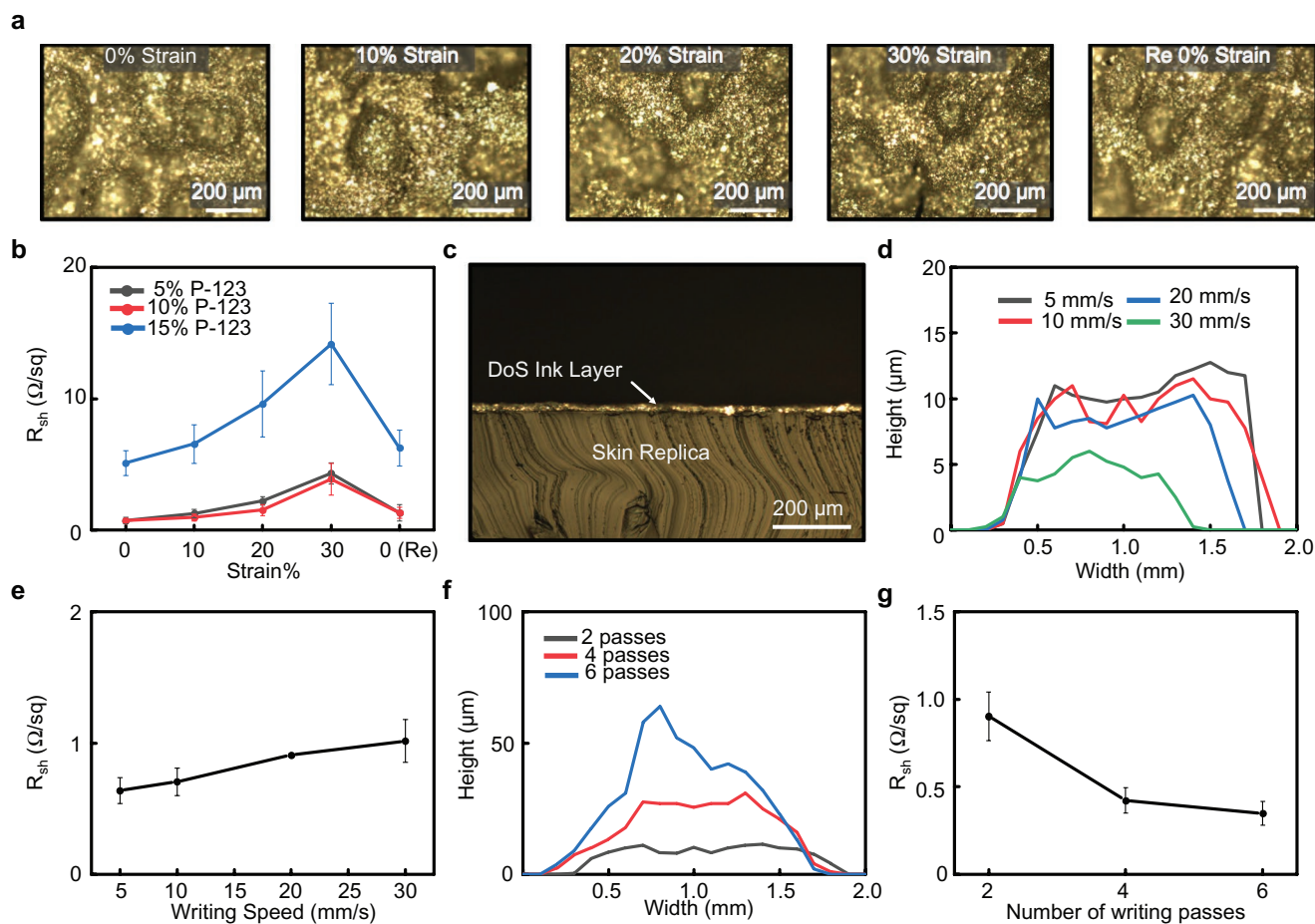
$$\eta(\gamma) = m\gamma^{n-1} \qquad (1)$$

where η is the viscosity, m is the consistency index associated with the magnitude of viscosity, γ is the shear rate, and n is the power-law index. The term n defines the viscosity behavior, where $n > 1$, $n = 1$, and $n < 1$ indicate shear thickening, Newtonian behavior, and shear thinning behaviors, respectively. The curve of ln η–ln γ was plotted based on the viscosity curves presented in Figure 1f, and by fitting the slope, the power-law index n of the inks was obtained. It was found that the power-law index n for DoS ink and the P123-modified PEDOT:PSS ink were ≈0.73 and ≈0.76, respectively. The n values of both inks were less than 1, indicating non-Newtonian fluids with shear thinning behavior. The larger the deviation of n from

1, the more non-Newtonian the behavior of the fluid. The resulting film's morphology from drawing with P123-modified PEDOT:PSS ink was investigated (Figure 1g,h). The atomic force microscope (AFM) phase image (Figure 1h) shows a distinctive PEDOT nanofibril network and PSS domains represented by bright and dark phases, respectively. It should be noted that an AFM image of the DoS ink could not be obtained due to the size of Ag flakes, which was on the order of a few micrometers. An optical microscopic image of the DoS ink on a skin replica is shown in Figure 1i, which shows the Ag flakes (bright spots).

2.2. DoS Material Optimization and Ink Drawing Characterizations

The conductive ink stretchability (10 wt% P123 in PEDOT:PSS solution) was tested over a PDMS-based skin replica (**Figure 2**a).

ADVANCED
SCIENCE NEWS
www.advancedsciencenews.com

NANO · MICRO
small
www.small-journal.com

Figure 2. a) Optical microscopic images of the DoS ink on skin replica stretched up to 30% and then back to 0%. b) Sheet resistance characterization for various P123 weight% for the drawn ink stretched from 0% to 30% and then back to 0% again ($n = 6$). c) Optical microscopic image of interface of the DoS ink with skin replica. d) Thickness profiles of drawn DoS ink at various speeds across the width of the drawn lines. e) Sheet resistance characterization of DoS ink for various writing speeds ($n = 6$). f) Thickness profiles for different numbers of writing passes across the width of the drawn lines. g) Sheet resistance characterization for number of writing passes ($n = 6$).

After drawing the ink over the skin replica, it was stretched from 0% to 30% and then back to 0%; minimum to no cracks were observed for all cases. This result supports the high conformality and stretchability of the conductive ink. Then the conductive ink was optimized for P123 weight percentage. To ensure the optimal ratio of P123 in PEDOT:PSS solution, 5, 10, and 15 wt% of P123 in PEDOT:PSS were evaluated in terms of sheet resistance from 0% to 30% strain and back to 0% strain. The results are shown in Figure 2b and Figure S1 in the Supporting Information. From all the weight percentages of P123 considered, 10 wt% of P123 in PEDOT:PSS was found to be the best performing case considering the sheet resistance at various strains. The sheet resistance increased from ≈0.71 Ω sq^{-1} at 0% strain to ≈3.88 Ω sq^{-1} at 30% strain and then decreased to ≈1.31 Ω sq^{-1} when the strain was released back to 0%. The increase in sheet resistance, when stretched from 0% strain to 30% strain, was attributed to the breakage in the PEDOT nanofibrils network as it was stretched (Figure S2, Supporting Information). The 5 wt% of P123 in PEDOT:PSS showed a higher increase in normalized sheet resistance, relative to that of the 10 wt% of P123 in PEDOT:PSS, as the applied strain was

increased (Figure S1, Supporting Information). For the 15 wt% of P123 in PEDOT:PSS, the overall sheet resistance was much higher relative to the other weight percentages considered. Higher weight percentages were not considered due to these factors and for the remainder of the work, only the 10 wt% of P123 in PEDOT:PSS was used. This ink is referred to as the DoS conductive ink when Ag flakes are added. Considering that the skin experiences repeated loading in daily activities, the aforementioned ink was evaluated on skin replica with a cyclical stretch and release test (Figure S1, Supporting Information). After 100 cycles of stretching at 10% and 30% strain, the resistance of the DoS conductive ink increased by a factor of 1.6 and 2, respectively. Next, we studied the effect of the writing parameters on the ink properties.

The optical microscopic image of the DoS ink layer thickness profile over the PDMS skin replica is shown in Figure 2c. At this magnification, the thickness profile is relatively uniform over the substrate. A closer examination of the effect of the writing speed on the height profile was performed (Figure 2d) using a profilometer. The lines were drawn at various speeds using a custom-built three-axis micropositioning system (Figure S3,

ADVANCED
SCIENCE NEWS
www.advancedsciencenews.com

NANO · MICRO
small
www.small-journal.com

Supporting Information). It was found that the height of the drawn lines for different writing speeds (5–30 mm s^{-1}) ranged from ≈12 to ≈6 µm, respectively. This indicates that there was not a substantial change in height as the writing speed increased. We then observed the effect of different writing parameters on the electrical properties of the ink. The sheet resistance for various writing speeds (Figure 2e) increased from ≈0.67 to ≈1 Ω sq^{-1} as the speed increased from 5 to 30 mm s^{-1}, which is in the range of handwriting speeds.[18] The effect of the number of writing passes over the same lines was also observed in terms of the height of the written lines and sheet resistance. The height of the written lines increased from ≈10 to ≈50 µm as we increased the writing passes from 2 to 6, as expected. The sheet resistance for increasing numbers of writing passes was found to decrease from ≈0.9 to 0.34 Ω sq^{-1}. It should be noted that a writing speed of 10 mm s^{-1} was utilized for this test. From all these results, it can be concluded that the writing parameters (writing speed and number of writing passes) do not have a substantial effect on the electrical performance of the conductive ink, which should minimize the variability of the sensor performance.

2.3. Cellular-, Tissue-, and Organ Level-Biocompatibility of the DoS Ink

In situ fabrication of devices with raw electronic materials requires biocompatibility from the cellular level to the tissue and organ levels, but it has yet to be thoroughly explored according to most of the current literature. We began the characterization of the cytocompatibility of the DoS conductive ink through in vitro culture (**Figure 3**a,b) of rat neonatal CMs over the course of 2 weeks. An electrode array pattern was drawn on tissue culture plate wells using the typical drawing process prior to seeding the cells, as shown in Figure S4 in the Supporting Information. Afterward, a few of the wells with an array pattern of the P123-modified PEDOT:PSS ink were coated with fibronectin to enhance cell attachment while others were left uncoated and only contained the exposed pattern. This step was repeated for the typical DoS conductive ink containing Ag. In all conditions (including the control), the elongated morphology of the CMs could be observed, even near the areas of the DoS conductive ink (Figure 3c). All the assays were performed with duplicates for each condition. It should be noted that if the experimental conditions showed similar cell viability or toxicity compared to the controls, the DoS ink is considered to be nontoxic. Cell viability tests further confirmed that across the DoS ink coated with fibronectin (Figure 3d), noncoated DoS ink (Figure 3e), and control samples (Figure 3f), there was a high cell viability (>95%). The population profiles showed (Figure S5, Supporting Information) similar distributions across all samples. The cell numbers were all within the same magnitude and the amount was similar to the initial seeding density (10^5 cells well^{-1}). Figure S6 in the Supporting Information shows that the corresponding cases for the P123-modified PEDOT:PSS ink produced similar viability results. Furthermore, to ensure that the stencil did not cause any toxicity issues, another condition in which the DoS conductive ink was drawn in an array pattern in the well, without a stencil, was compared in terms of the cell

viability and population profile (Figure S7, Supporting Information). As expected, there is no residual toxic material from the stencil that substantially affects the cell viability. A lactate dehydrogenase assay (LDH) was performed to investigate the toxicity of the material. Generally, an increasing cell number corresponds with a higher LDH activity, which can be observed in Figure S8 in the Supporting Information, but the toxicity level remained low overall for all conditions. It should be noted that for all the tested conditions, throughout the 2 weeks, regular CM contractions could be consistently observed after 6 d of culture. To evaluate the compatibility of the DoS ink with another cell type, similar tests were conducted using rat cortical neurons for cell viability (Figure S9, Supporting Information) and toxicity (Figure S10, Supporting Information). Again, the DoS conductive ink showed no harmful effect to the cells. These results indicate that our ink is compatible with multiple critical cell types and could potentially be utilized for making DoS devices and sensors directly on target organs, such as the heart and the brain.

The multiday biocompatibility of the DoS ink at the tissue level was studied using mice to determine the presence of inflammation in the dermal and epidermal layers of the skin. The conductive ink was drawn in lines on the back of CD1 mice and monitored for 3 d. Compared to the control (no ink) condition, the DoS ink condition showed little to no inflammation over all 3 d in the hematoxylin and eosin (H&E) staining images (Figure 3g–i). The immune cells in the images were counted from 5 high power fields (HPF) and showed no statistically significant differences between the two conditions, as shown in Figure S11 in the Supporting Information. An additional assay was performed to observe the presence of inflammatory cytokines, such as interleukin-6 (IL-6) and interleukin-10 (IL-10), both of which are markers for dermatitis (Figure S11, Supporting Information). By analyzing several HPFs, the pathologist determined that they were no statistically significant differences between the DoS ink and control conditions over all 3 d, for both IL-6 and IL-10. Finally, the DoS ink was tested on human skin for irritation after multiple times of drawing in the same location for ECG measurements (**Figure 4**a). Due to the reconfigurable nature of DoS electronics, the DoS sensor could be repeatedly drawn and then rubbed off (using a wet paper towel), leaving no redness or visible skin irritation even after ten repeated rubbings (Figure 4b,c). The skin histology and human skin tests further prove that the raw components of the DoS ink are fully biocompatible, which makes them suitable for various applications on the human skin, including multiple types of electrophysiology.

2.4. DoS Sensor and Wiring Scheme

Several critical health parameters can be gleaned from the skin surface including ECG, EMG, EEG, and EOG signals. To capture these signals, the DoS ink was utilized as an EP sensor. The connection scheme is pictured in Figure 4d, which shows the DoS sensor, DoS interconnect, medical tape, and wire to the data acquisition (DAQ) system. The interconnect was insulated from the skin using liquid bandage that was applied to the skin in a similar manner to that of the DoS ink. The drawing and
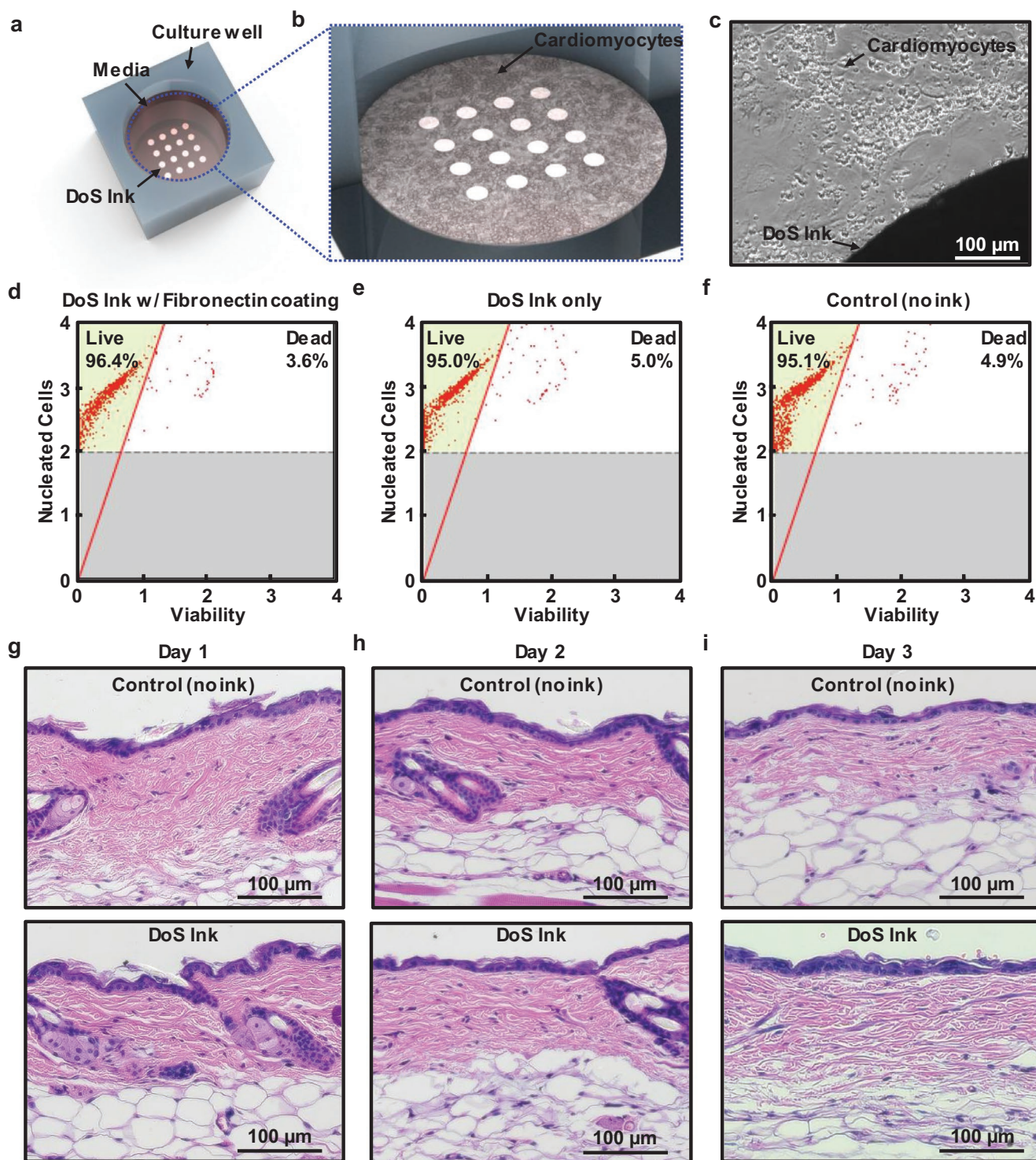
Figure 3. a) Schematic of the cardiomyocytes cultured on DoS ink in a culture well. b) Zoomed-in view showing in-plane growth of CMs over the entire well and around DoS ink. c) Optical microscopic image of CMs next to one of the DoS ink patterns. d) Viability profile of CMs cultured on the DoS ink covered with fibronectin coating. e) Viability profile of CMs cultured on DoS ink covered without any matrix coating. f) Viability profile of CMs cultured on the fibronectin-coated wells. Histology images of the control (top) mouse skin and DoS ink (bottom) covered mouse skin conditions on g) day 1, h) day 2, and i) day 3.

connection process is as follows. First, a stencil for the interconnect was placed on the skin and the liquid bandage was drawn. After a few minutes, the liquid bandage dried, and the interconnect stencil was removed. Next, another stencil containing the outline of both the interconnect and DoS sensor was placed over the dried liquid bandage. The DoS ink was
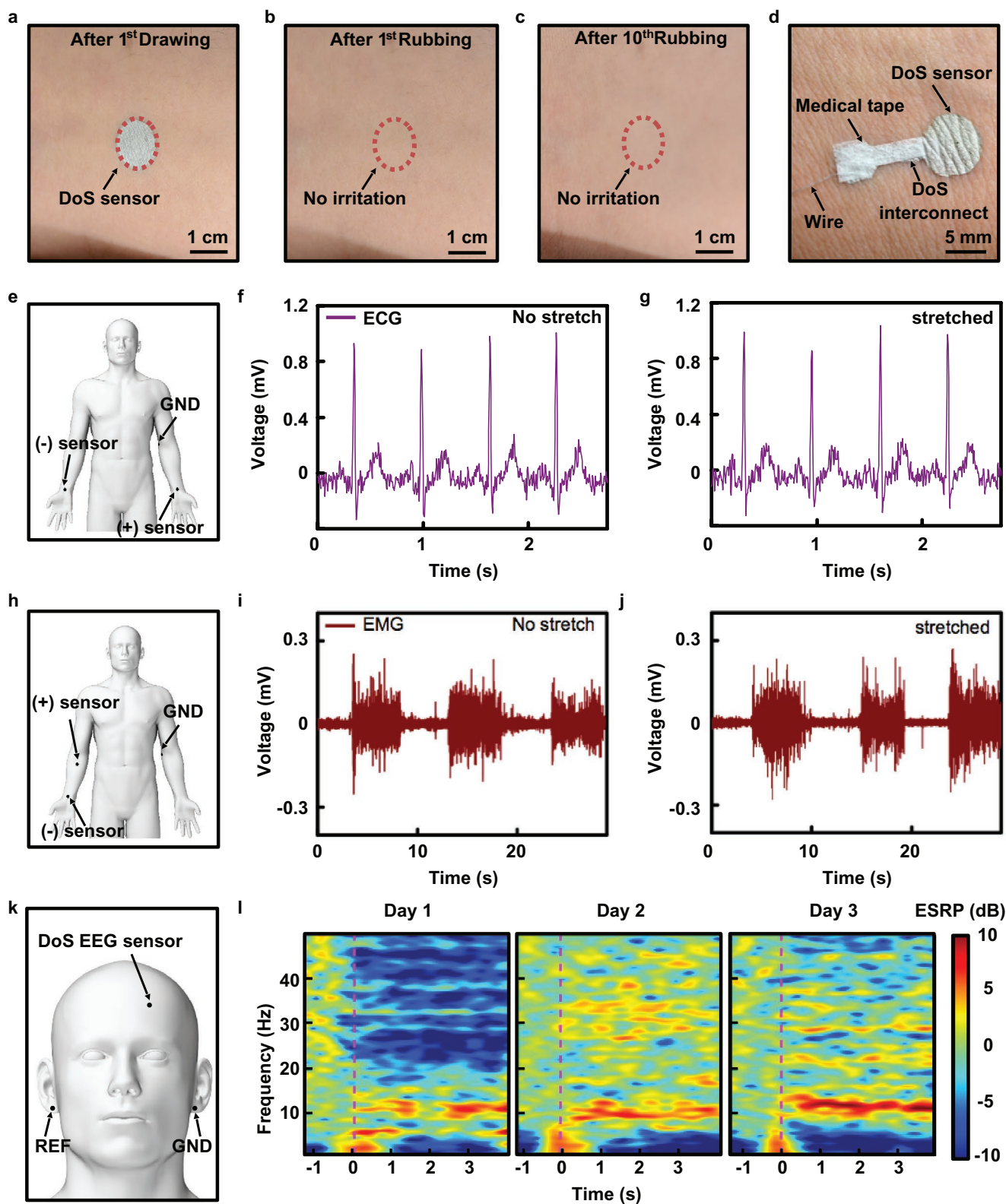
Figure 4. a) DoS sensor on the wrist of a human subject. b) DoS sensor after rubbing off one time, showing no irritation. c) DoS sensor after redrawing and rubbing off ten times, still showing no irritation. d) Connection and interface setup for DoS sensors. e) Schematic for ECG measurement. ECG signals recorded with f) no strain placed on the DoS sensor and g) ≈10% strain. h) Schematic for EMG measurement. EMG signals recorded with i) no strain placed on the DoS sensor and j) ≈10% strain. k) Schematic for EEG measurement. l) Time-frequency maps over 3 d measurement of the alpha rhythm during mental relaxation (subject closed his eyes).

ADVANCED
SCIENCE NEWS
www.advancedsciencenews.com

NANO · MICRO
small
www.small-journal.com

drawn into the outline of the entire stencil. Both of the stencils are shown schematically in Figure S12 in the Supporting Information. About 5 min of drying time was required for the film to appear mostly dry and then the stencil for the DoS ink was removed. To connect the sensor to the DAQ, a thin stainless-steel wire (insulated) was stripped to expose the conductive core and then placed onto the end of the DoS interconnect (i.e., contact pad). This stainless-steel wire was chosen since it is flexible and almost imperceptible to the user, making it comfortable for the subject. Medical tape, cut into the shape of the DoS interconnect, was placed on the wire to secure it to the sensor. The adhesion of the medical tape is strong enough to hold the wire in place, even when the wire is slightly tugged. The force over time to detach the tape and wire from human skin is shown in Figure S13 in the Supporting Information. Additionally, the adhesion of the DoS ink to the skin was evaluated (Figure S13, Supporting Information). After applying tape to the sensor (Magic Tape, 3M) and removing it, little to no damage could be observed. To continue the connection setup, another layer of DoS ink was drawn on top of the interconnect region of the medical tape, to sandwich the wire in the conductive ink. A cross-sectional schematic of this setup is provided in Figure S14 in the Supporting Information. In addition, optical microscope images were obtained to verify that the DoS ink can penetrate the medical tape, from the nonadhesive side to the adhesive side of the tape. As shown in Figure S15 in the Supporting Information, the microscope image of the nonadhesive side shows distinct fibers of the tape and the Ag flakes of the DoS ink. The interface between the tape fibers and DoS ink can be easily distinguished by comparing the brightness of the respective regions. The tape fibers are long (on the order of centimeters) and are tens of micrometers wide. The DoS ink sinks into the gaps between the fibers and also sits on them. On the adhesive side, the Ag regions are not as distinguishable, but they can still be observed in some regions of the tape. Again, the overall brightness of the image showing the adhesive and DoS ink is still higher compared to that of the adhesive only. Furthermore, there are open pores that can be observed on the adhesive side without the DoS ink, whereas the pores all appear filled in the opposite case. Two-point resistance measurements were briefly performed to verify that the resistances on both sides of the tape were similar to those reported in Figure 2b. These results clearly suggest that the DoS ink penetrates from the top nonadhesive side of the tape to the bottom adhesive of the tape, creating a conductive pathway in the z-direction and forming a robust electrical connection to the DAQ. The quality of the DoS ink as an EP sensor was evaluated in the following.

2.5. DoS Sensor for ECG and EMG Sensing

EP signals with high signal-to-noise ratios (SNRs) substantially contribute to the accuracy of medical diagnosis.[19] We characterized the quality of the DoS EP sensors by first determining their impedance characteristics over physiologically relevant frequencies. The impedance of a 7 mm diameter DoS sensor was measured using electrical impedance spectroscopy and the low impedance in the frequency range <100 Hz (Figure S16, Supporting Information) indicates the DoS sensor is suitable

for high fidelity measurements.[20–23] In addition, compared to the traditional gel electrodes, the DoS sensors have a normalized impedance that is in the same order of magnitude, which is not normally the case for metal-based electrodes. We then measured some of the pertinent EP signals that can be obtained from the skin beginning with ECG signals, which reveal information about the health of the heart's conduction system and evaluated their quality. The recording setup shown schematically in Figure 4e was used to capture ECG signals from the wrists of a human subject. Camera images of the device on the skin are provided in Figure S17 in the Supporting Information. The signals shown in Figure 4f,g show the ECG signals captured without applied strain to the sensor and with strain ($\varepsilon \approx 10\%$), respectively. In both cases, all parts of the ECG waveform including the P, QRS, and T sub-waves are clearly observable. The calculated SNR of the ECG signals for both without and with applied strain cases were 44.45 and 44.36 dB, respectively. Customizing DoS sensors to various muscle anatomies of different individuals could reveal underlying muscle activity and provide improved signal quality.[24–26] Thus, EMG signals were recorded from the flexor carpi radialis muscle of the forearm (Figure 4h). In both the without applied strain (Figure 4i) and with strain ($\varepsilon \approx 10\%$) cases (Figure 4j), the bursts of muscle activity obviously stand out relative to the baseline, which indicates that the summed motor unit activity could be successfully captured. The average baseline noise was in the range of $\pm$ 20 µV. It should be noted that minimal filtering was applied (mainly to remove power line noise or keep the relevant signal frequency band) for the ECG and EMG signals. The calculated SNR of the EMG signals for both without and with applied strain cases were 31.29 and 30.22 dB, respectively. These results indicate that the DoS EP sensors can evidently capture ECG and EMG signals with high SNRs.

2.6. DoS Sensor for EEG Multiday Sensing

The various frequency bands of EEG signals including delta (0–4 Hz), theta (4–8 Hz), alpha (8–13 Hz), beta (13–30 Hz), and gamma bands (>30 Hz),[27] can reveal various dynamic states of the human brain. In particular, the alpha frequency band has been used to study motor intent and motor execution, mental relaxation, and sleep stages.[28] Here, we demonstrate the first multiday test of in situ fabricated sensors for EEG recording. The DoS EP sensor was drawn on the forehead in the Fp1 position of the standard 10–20 placement system and the setup is schematically shown in Figure 4k. On each day over the course of the 3 d test, the subject visited the lab at the same time of day to have their EEG signals recorded and continuously wore the sensors while performing his daily routines outside of the lab, including face washing, sleeping, and running. It should be noted that EEG signals were not recorded while the subject was outside of the lab. Prior to the measurements, the medical tape over the DoS interconnect was lifted and the wire was inserted underneath. Then an additional layer of ink was drawn on top of the interconnect section over the tape to encapsulate the wire in DoS ink. During the recording, the subject was instructed to close his eyes for 20 s and open them for 10 s; this was repeated for a total of 18 trials. The average spectrograms of all trials,

based on each day, are shown in Figure 4l. In each spectrogram, the purple dashed line indicates the start of the trial or the "eyes closed" event. As expected, the alpha power sharply increased after the subject closed his eyes and this is indicated by the orange and red color between 8 and 13 Hz in the spectrograms. It should be noted that the higher frequencies on day 1 were more silent, relative to the target signal. On day 2 and day 3, the alpha rhythms were clearly captured although there is more higher frequency activity across the rest of the spectrograms. The calculated SNRs for day 1, day 2, and day 3 were 5.82, 4.83, and 5.18 dB, respectively. The power spectral density for each day is plotted in Figure S18 in the Supporting Information and a wide peak can be observed across the alpha band on all days.

In addition to evaluating the signal quality, the appearance of the sensor and medical tape were examined each day. On the first day, the medical tape was applied to the entirety of the sensor to fully protect it and a layer of ink was drawn on top of the interconnect portion of the tape (Figure S19, Supporting Information). On the second day, the tape appears darker, likely from having absorbed some water (the subject washed his face) and the portions of the ink on top of the tape rubbed off. Again, the ink was drawn onto the interconnect portion of the tape immediately prior to the measurement. The tape appears a bit darker on day 3, though the ink on the tap had not rubbed off as much as it did on day 2 (Figure S19, Supporting Information). To check the DoS sensor underneath the electrode after the day 3 measurement, the tape was removed and photographed, as shown in Figure S19 in the Supporting Information. The adhesive side (bottom side interfaced with the skin) showed partial removal of the DoS sensor from the skin surface, though remnants of the sensor were still visible on the forehead of the subject. This indicates that the DoS sensor forms into a film that can be peeled off after the end of the usage period. The remaining portions of the film can be easily removed with a wet paper towel. The high SNR of the EEG signals across multiple days and the physical robustness of the sensor and connection scheme are promising for multiday monitoring of EP signals.

2.7. DoS Sensor for EOG-Controlled Human–Machine Interface

The corneoretinal standing potential created between the front and back of the eye is a commonly used signal to determine the eye's position.[19] EOG signals have been implemented in several control applications as the signals can be differentiated for classifying different movements.[29–31] Our bipolar measurement setup shown in **Figure 5**a was used to record both the horizontal (hEOG) and vertical (vEOG) eye movements. The hEOG channel (Figure 5b) clearly showed positive or negative deflections, based on left and right eye movements (respectively), which are determined by the polarity of the bipolar channel. Since the positive sensor was placed near the left eye, when the subject shifted his gaze to the left, a positive deflection was observed and maintained at around 600 µV until the subject shifted his gaze back to a central position. It should be noted that the vEOG channel during the left and right eye movements shows a substantially lower amplitude, which makes it simple to identify a left/right eye movement with just the hEOG channel. A similar, but opposite shape was

observed when the subject shifted his gaze to the right in the hEOG channel (bottom left curve). The signals recorded with the vEOG channel were like that of the hEOG channel but were more obvious when the subject looked down (top right curve) or up (bottom right curve). Again, minimal postprocessing was used and details are included in the Experimental Section. Since each signal from looking left, right, up, and down is unique to each channel, the signals could potentially be used for a highly accurate HMI to control various objects, such as wheelchairs, drones, or virtual game characters.[31–34] A custom maze game with a virtual character was developed to serve as an example of an eye movement-controlled HMI (Figure 5c). To enable near real-time control, a simple program was made in MATLAB to identify the different eye movements. The subject controlled the blue cube through the paths with their eye movements to obtain collectables (green cylinders) and escape the maze. These results indicate that the DoS EOG sensors could easily be utilized for virtual reality applications and other HMIs.

3. Conclusion

We demonstrated the first fully biocompatible, on-site fabricated electronics for multiple cell types and tissues that can capture EP signals with high fidelity. The mechanical stretchability and conductivity are improved relative to the previous report as the ink can still maintain a low sheet resistance under 30% strain, while being made from all biocompatible electronic materials. The writing characterization reveals that variability of handwriting does not substantially affect the mechanical and electrical properties of the ink. In vitro cell viability and toxicity assays with primary CMs and neurons prove the cellular level biocompatibility of the ink. The inflammation-free skin tissue stains and irritation-free human skin demonstrate both tissue level and multiday organ level biocompatibility, respectively. Finally, the high-SNR EP signals, multiple days of monitoring, and eye movement-controlled HMI demonstrate that the robust connection setup and DoS sensors could be viably implemented for continuous and personalized ambulatory monitoring of wounds, skin, and other organs in future studies.

4. Experimental Section

Materials: Ag flakes (10 µm size, 99.9% trace metals basis, 327077) and poly(ethylene glycol)-*block*-poly(propylene glycol)-*block*-poly(ethylene glycol) (Pluronic P-123, 435465) were purchased from Sigma-Aldrich and used without further modification. PEDOT:PSS (PH 1000) was from Ossila Limited. PDMS rubber (Sylgard 184 Silicone Elastomer Kit) was from Dow Corning.

Conductive Ink Preparation: The DoS conductive ink was prepared by first making the highly conductive PEDOT:PSS solution and then adding in the Ag flakes. First, the PEDOT:PSS solution was prepared by stirring 5, 10, and 15 wt% P-123 into the commercial PEDOT:PSS solution for 12 h at room temperature (≈22 °C) at 800 rpm. Afterward, the prepared solution was stored at ≈4 °C in a refrigerator. Prior to adding Ag flakes, the PEDOT:PSS solution was taken out of refrigerator and stirred for 1–2 min. Then the corresponding amount of Ag flakes (1:2 weight ratio, Ag flakes: PEDOT:PSS solution) in the form of powder was added to the vial, the PEDOT:PSS solution was added to the vial and the mixture was stirred on a magnetic stirrer for about 1 h. The resulted ink was ready to
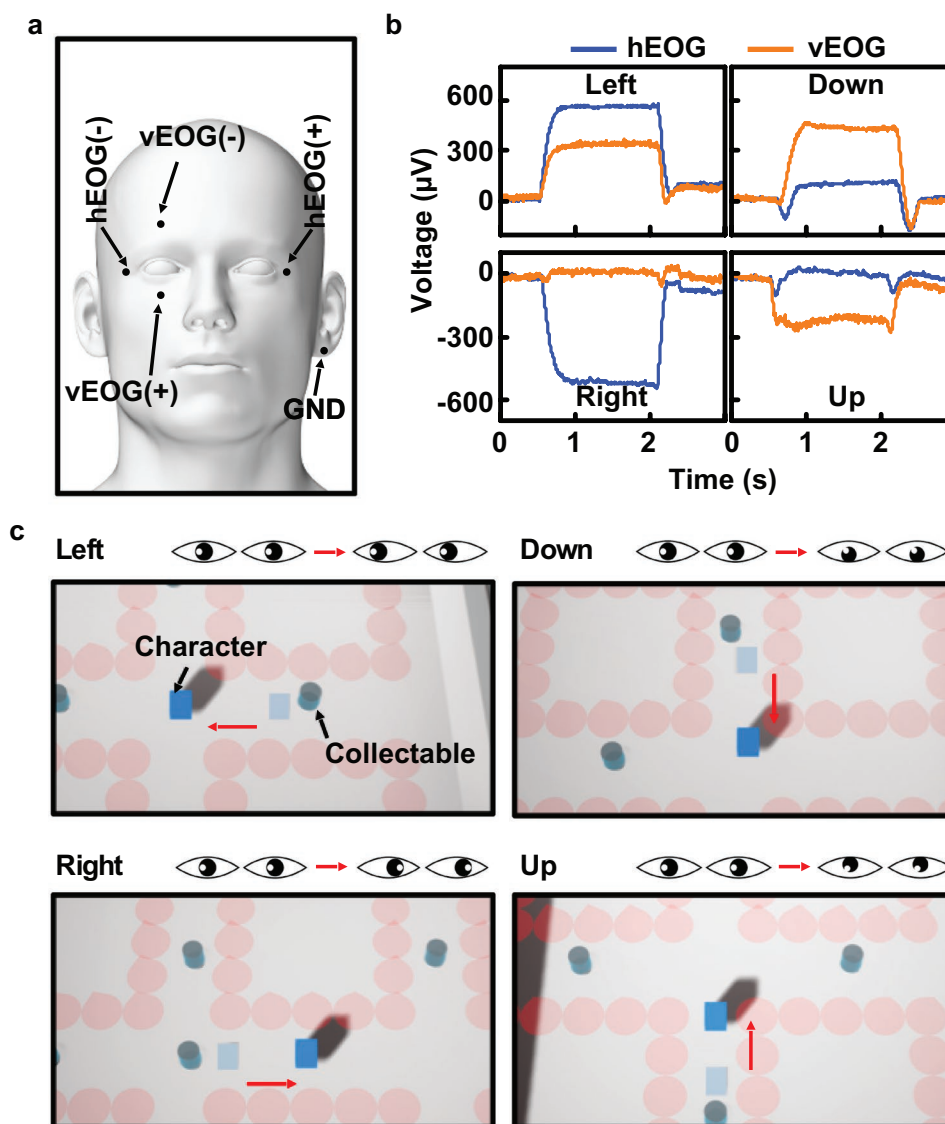
Figure 5. a) Schematic for EOG measurement. b) EOG signals from horizontal (hEOG) and vertical (vEOG) channels when the subject looked left, down, up, or right. c) Virtual game character (blue cube) controlled by the subject's eye movements to gather the collectables (green cylinders) and escape the maze.

use after the stirring, but it could be stirred more if any visible Ag flakes powder was remaining. The 10 wt% P-123 in PEDOT:PSS showed the optimal combination of low resistance and minimal resistance change after mechanical stretching, as shown in Figure S1 in the Supporting Information.

Ballpoint Pen Preparation: Ballpoint pens (557154012, PEN + GEAR) were fully disassembled. The balls from the pen tips and the original inks were removed. The tips and ink barrels were thoroughly cleaned in acetone, sonicated in deionized water, and air dried. Then, the ink was injected into the emptied ink barrels via a syringe and 26-gauge needle.

Ink Rheology: A TA Instrument (Discovery HR-2) was used to analyze the dynamic rheological characteristics. The rheology equipment parameters for the required test using the cone-plate geometry were as follows: angle of the cone, gap distance between the plates. The test performed at 25 °C using a water bath. In the flow sweep test, the shear rates were 1–1000 s⁻¹. Three samples were tested per condition (PEDOT:PSS with P123 and DoS conductive ink).

PDMS Skin Replica Preparation: The PDMS solution was prepared by mixing the prepolymer/curing agent at the weight ratio of 10:1. Porcine

skin was purchased from a grocery store and cut into pieces. On the dermis of the skin, epoxy adhesive was applied and attached to a piece of Kapton tape. The epoxy secured the porcine skin to the tape and ensured that skin did not shrivel too much at ambient conditions. Uncured PDMS mixture was poured into a petri dish. The porcine skin pieces attached to the Kapton tape were flipped over such that the epidermis was facing down and gently submerged into the uncured PDMS. This ensured that the PDMS was thin enough for mechanical characterization. They were left to cure at room temperature for 2 d. Afterward, the petri dish was put into a curing oven (≈80 °C) for 1 h. After curing, the PDMS was cut and the molds were separated from the porcine skin. Surface treatment of the skin replica was performed using UV/O₃ for 6 min and then submerging in (3-aminopropyl)triethoxysilane (APTES) for 20 min.

Test Sample Preparation for Characterization: The DoS electronics drawing process[10] was used to prepare the test samples with the pen writing speed being manipulated by a three-axis micropositioning system (custom-built 3D printer) at room temperature on a PDMS substrate. Before the test sample was drawn over the PDMS substrate,

surface treatment of the PDMS substrate was performed using UV/O$_3$ for 6 min and then submerging in 1% APTES solution for 20 min. Afterward, the treated substrate was placed on the bed of the three-axis micropositioning system and the pen was fixed to the printhead. The drawing process was started with the software (Pronterface) at different speeds (5, 10, 20, 30 mm s^{-1}) and each line was drawn accordingly on the substrate. Average dimensions of each sample (rectangle-shaped) were 45 mm in length and 1.5 mm in width. The samples were left to dry in ambient conditions for 5 min.

Characterization of Test Sample: Flat PDMS substrate was prepared in a similar way as described in skin replica preparation. The Ag-PEDOT:PSS ink was drawn onto the flat PDMS substrate for mechanical characterization. The SEM (XL-30S FEG, Philips) and AFM (Dimension Icon, Bruker) images were taken to observe the morphologies and skin confirmability of the ink respectively. Optical microscope images were taken with the Nikon Eclipse LV100ND. Electrical resistance was measured using a Keithley DMM6500 6 1/2 Digit Multimeter and two-point measurement. Sheet Resistance was calculated by dividing the resistance with the number of squares. The test sample used here was 45 mm in length and 1.5 mm in width. Hence, the number of squares in the test sample was 30. The thickness of the test sample drawn was measured using Profilometer (Tencor Instruments AS-266). Stretching/releasing tests were performed with a cyclic automatic stretcher (CK-700FET, CKSI Co. Ltd.). Measurements were taken after the sample returned to 0% strain.

Cardiac and Neuron Cell Viability: Cell viability and count was determined using laser-based fluorescence detection via the Muse instrument and Muse (Luminex Corporation). A count and viability Assay Kit stain (Catalog: MCH600103, Millipore Sigma) was performed by following the manufacturer's protocols. Briefly, after passing the quality control of the instrument, 20 µL of uniform cell suspension was added into 380 µL of the count and viability assay kit, followed by 5 min of incubation in the dark at room temperature, and then the samples were run on the Muse cell analyzer.

Cardiac and Neuron Cell Toxicity: Cytotoxicity was assessed by quantitively measuring LDH, a stable cytosolic enzyme that is released upon cell lysis. The CytoTox-ONE Homogeneous Membrane Integrity Assay (catalog: G7890, Promega) was used by following the manufacturer's protocols. Briefly, frozen cell culture supernatant was thawed for quantification. Then, 100 µL of the cell culture supernatant from each sample was placed in a 96-well plate, and 100 µL of CytoTox-ONE reagent was added to each well. The plate was mixed for 30 s and incubated for 10 min while being protected from light. Next, 50 µL of stop solution was added to each well of the 96-well plate and fluorescence with an excitation wavelength of 560 nm and an emission of wavelength of 590 nm was recorded using an Infinite 200 PRO plate-reader (Tecan). Assays were performed in triplicate for all samples.

Skin Histology: First, three Cd-1 mice were anesthetized with isoflurane. Dorsal hair was removed with hair removal cream. On day 0, the conductive ink was drawn on the back of the mice. On days 1, 2, and 3, samples of the skin with and without ink (control) were harvested. All conditions were tested in duplicate. The tissue samples were fixed in formalin and embedded in paraffin. H&E stain was utilized for the histology. Images shown were all taken from the same mouse. All procedures followed the National Institutes of Health Guide for the Care and Use of Laboratory Animals and were approved by the University of Chicago Institutional Animal Care and Use Committee (Protocol 72219).

Cytokine Immunohistochemistry Assay: Paraffin-embedded and formalin-fixed skin sections were stained on a Leica Bond RX automatic stainer. Epitope retrieval solution II (Leica Biosystems, AR9640) was used for 20 min heat induced antigen retrieval treatment. Anti-IL-6 antibody (Proteintec #21865-1, 1:800) and anti-IL-10 antibody (Proteintec #20850-1, 1:1500) were applied on tissue sections, incubated for 60 min, and the antigen-antibody binding was detected with the Bond polymer refine detection (polymer horse radish peroxidase, Leica Biosystems, DS9800). A section from mouse spleen was used as a positive control. For quantification, slides were inspected under the microscope at high power (400x magnification) and intradermal cells with IL-6 or IL-10

staining were counted manually by a trained pathologist. For each slide, 8–10 random fields were inspected. All conditions were tested in duplicate.

Force Measurement: The medical tape (Nexcare, gentle paper tape) was adhered to the bicep of the subject. For the "tape only" condition, the tape was marked such that only a 5 mm length of the tape remained attached to the skin, and another piece of tape was used to attach to the excess after the 5 mm mark. The other piece of tape was clamped to a force gauge setup (Mark-10 with digital force gauge Series 5). For the "wire under tape" condition, the wire (5 mm length) was fixed onto a subject's skin with a 5 mm tape. The wire was clamped to the force gauge setup.

Skin to Electrode Impedance: The skin impedance was measured using an impedance analyzer (Multi/Autolab M204, Metrohm) connected to two DoS sensors placed in the ECG measurement configuration (wrists only) shown in Figure 4e. The DoS sensors were 7 mm in diameter. The impedance was measured from 1000 to 1 Hz. For comparison, a hospital-grade gel electrode was also tested.

ECG and EMG Measurements and SNR Calculations: The schematics of the setups are shown in Figure 4e,h for ECG and EMG, respectively. The subject had his skin wiped with isopropyl alcohol. The DoS sensors were 7 mm in diameter. Measurements were taken with a Recording Controller (Intan Technologies) and amplifier board (RHD2216). A sampling rate of 2000 Hz was utilized. For postprocessing, both ECG and EMG signals were filtered with only a 3rd order Butterworth, 1 Hz high-pass filter and 60 Hz notch filter. To calculate the SNR for each of the sensor types, first the power spectral density estimate was obtained using Welch's method in MATLAB. The parameters for the pwelch function were chosen to be a 2000-point Hanning window (i.e., the sampling frequency) and a 50% overlap. The noise was averaged from the region obviously in the noise floor. The following formula was used to convert the ratio of the signal and noise to power in dB

$$SNR = 10 \times \log_{10} \frac{P_{(s)}}{P_{(n)}} \tag{2}$$

where $P_{(s)}$ is the power of the signal and $P_{(n)}$ is the power of the noise.

EEG Measurements: The schematic of the setup is shown in Figure 4k. An OpenBCI Cyton board was used to acquire data at a sampling rate of 250 Hz. The data were filtered in MATLAB with a 3rd order Butterworth bandpass filter (0.5–50 Hz) and a 60 Hz notch filter. Time-frequency analysis was performed using EEGLAB. SNR calculations followed the same approach as described in the previous section. All the procedures were approved by the Institutional Review Board of the University of Houston, TX (USA) and informed consent was obtained (Protocol 2765).

EOG Measurements and Game Application: The schematic of the setup is shown in Figure 5a. The same OpenBCI system was used. The data were filtered only with a 60 Hz notch filter, similar to that of the previous signals. The game was developed in Unreal Engine (Epic Games). A MATLAB script was written to read in real-time EOG data and make a prediction every 2 s for the user's eye movement (left, right, up, down, or no movement). An Arduino program was written and loaded onto a microcontroller (Arduino Micro) to send the prediction from the MATLAB to a keyboard press (left, right, up, down arrows, or space bar). These commands from the keyboard could be read by the game.

Statistical Analysis: For the viscosity measurement against shear rate, sheet resistance characterization of ink for various P123 weight% in ink, sheet resistance characterization of ink for various writing speed, sheet resistance characterization for increasing number of writing passes, cell viability, cytotoxicity, histology, and immunohistochemistry tests, no data preprocessing was performed. Data are presented as mean ± standard deviation with a sample size of $n = 3$ for cell viability, cytotoxicity, histology, and immunohistochemistry tests, $n = 4$ for viscosity measurement against shear rate and $n = 6$ for sheet resistance characterization of ink for various P123 weight% in ink, sheet resistance characterization of ink for various writing speed and sheet resistance characterization for increasing number of writing passes. An unpaired Student's *t*-test was performed for cell viability, cytotoxicity, histology, and immunohistochemistry tests, with a *p*-value

<0.05 considered as significant. GraphPad Prism (8.0.1) was used for statistical analysis and generating the graphs.

Supporting Information

Supporting Information is available from the Wiley Online Library or from the author.

Conflict of Interest

The authors declare no conflict of interest.

Data Availability Statement

The data that support the findings of this study are available from the corresponding author upon reasonable request.

[1] X. Huang, Y. Liu, G. W. Kong, J. H. Seo, Y. Ma, K. I. Jang, J. A. Fan, S. Mao, Q. Chen, D. Li, H. Liu, C. Wang, D. Patnaik, L. Tian, G. A. Salvatore, X. Feng, Z. Ma, Y. Huang, J. A. Rogers, *Microsyst. Nanoeng.* **2016**, *2*, 16052.

[2] J. H. Kim, S. R. Kim, H. J. Kil, Y. C. Kim, J. W. Park, *Nano Lett.* **2018**, *18*, 4531.

[3] L. M. Ferrari, U. Ismailov, J.-M. Badier, F. Greco, E. Ismailova, *npj Flexible Electron.* **2020**, *4*, 1.

[4] Z. Zhu, S. Z. Guo, T. Hirdler, C. Eide, X. Fan, J. Tolar, M. C. McAlpine, *Adv. Mater.* **2018**, *30*, 1707495.

[5] N. X. Williams, S. Noyce, J. A. Cardenas, B. Catenacci, B. J. Wiley, A. D. Franklin, *Nanoscale* **2019**, *11*, 14294.

[6] L. Lin, M. Dautta, A. Hajiaghajani, A. R. Escobar, P. Tseng, M. Khine, *Adv. Electron. Mater.* **2020**, *7*, 2000765.

[7] A. Martin, C. Du, A. M. Pauls, T. Ward, M. Thuo, *Adv. Mater. Interfaces* **2020**, *7*, 2001294.

[8] L. Zhang, H. Ji, H. Huang, N. Yi, X. Shi, S. Xie, Y. Li, Z. Ye, P. Feng, T. Lin, X. Liu, X. Leng, M. Li, J. Zhang, X. Ma, P. He, W. Zhao, H. Cheng, *ACS Appl. Mater. Interfaces* **2020**, *12*, 45504.

[9] A. J. Bandodkar, W. Jia, J. Ramirez, J. Wang, *Adv. Healthcare Mater.* **2015**, *4*, 1215.

[10] F. Ershad, A. Thukral, J. Yue, P. Comeaux, Y. Lu, H. Shim, K. Sim, N. I. Kim, Z. Rao, R. Guevara, L. Contreras, F. Pan, Y. Zhang, Y. S. Guan, P. Yang, X. Wang, P. Wang, X. Wu, C. Yu, *Nat. Commun.* **2020**, *11*, 3823.

[11] H. He, L. Zhang, X. Guan, H. Cheng, X. Liu, S. Yu, J. Wei, J. Ouyang, *ACS Appl. Mater. Interfaces* **2019**, *11*, 26185.

[12] J. H. Lee, Y. R. Jeong, G. Lee, S. W. Jin, Y. H. Lee, S. Y. Hong, H. Park, J. W. Kim, S. S. Lee, J. S. Ha, *ACS Appl. Mater. Interfaces* **2018**, *10*, 28027.

[13] A. Giuri, S. Masi, S. Colella, A. Listorti, A. Rizzo, A. Kovtun, S. Dell'Elce, A. Liscio, C. E. Corcione, *Polym. Eng. Sci.* **2017**, *57*, 546.

[14] F. Zabihi, Y. Xie, S. Gao, M. Eslamian, *Appl. Surf. Sci.* **2015**, *338*, 163.

[15] A. Ankhili, X. Tao, C. Cochrane, V. Koncar, D. Coulon, J. M. Tarlet, *Sensors (Basel)* **2019**, *19*, 416.

[16] F. A. Morrison, *Understanding Rheology*, Oxford University Press, New York **2001**.

[17] B. Zhang, S. H. Chung, S. Barker, D. Craig, R. J. Narayan, J. Huang, *Prog. Nat. Sci.: Mater. Int.* **2021**, *31*, 180.

[18] S.-M. Jeong, T. Lim, J. Park, C.-Y. Han, H. Yang, S. Ju, *Nat. Commun.* **2019**, *10*, 4334.

[19] Y. Liu, M. Pharr, G. A. Salvatore, *ACS Nano* **2017**, *11*, 9614.

[20] K. Zhu, W. Guo, G. Yang, Z. Li, H. Wu, *ACS Appl. Electron. Mater.* **2021**, *3*, 1350.

[21] K. J. Yu, D. Kuzum, S.-W. Hwang, B. H. Kim, H. Juul, N. H. Kim, S. M. Won, K. Chiang, M. Trumpis, A. G. Richardson, H. Cheng, H. Fang, M. Thompson, H. Bink, D. Talos, K. J. Seo, H. N. Lee, S.-K. Kang, J.-H. Kim, J. Y. Lee, Y. Huang, F. E. Jensen, M. A. Dichter, T. H. Lucas, J. Viventi, B. Litt, J. A. Rogers, *Nat. Mater.* **2016**, *15*, 782.

[22] W. Lee, S. Kobayashi, M. Nagase, Y. Jimbo, I. Saito, Y. Inoue, T. Yambe, M. Sekino, G. G. Malliaras, T. Yokota, M. Tanaka, T. Someya, *Sci. Adv.* **2018**, *4*, eaau2426.

[23] A. Miyamoto, S. Lee, N. F. Cooray, S. Lee, M. Mori, N. Matsuhisa, H. Jin, L. Yoda, T. Yokota, A. Itoh, M. Sekino, H. Kawasaki, T. Ebihara, M. Amagai, T. Someya, *Nat. Nanotechnol.* **2017**, *12*, 907.

[24] Y. Xu, G. Zhao, L. Zhu, Q. Fei, Z. Zhang, Z. Chen, F. An, Y. Chen, Y. Ling, P. Guo, S. Ding, G. Huang, P. Y. Chen, Q. Cao, Z. Yan, *Proc. Natl. Acad. Sci. U. S. A.* **2020**, *117*, 18292.

[25] S. Gandla, H. J. Chae, H.-j. Kwon, Y. C. Won, H. Park, S. Lee, J. Song, S. Baek, Y.-D. Hong, D. H. Kim, S. Kim, *IEEE Trans. Ind. Electron.* **2021**, *69*, 4245.

[26] S. Velasco-Bosom, N. Karam, A. Carnicer-Lombarte, J. Gurke, N. Casado, L. C. Tome, D. Mecerreyes, G. G. Malliaras, *Adv. Healthcare Mater.* **2021**, *10*, 2100374.

[27] T. Harmony, *Front. Integr. Neurosci.* **2013**, *7*, 1.

[28] R. Abiri, S. Borhani, E. W. Sellers, Y. Jiang, X. Zhao, *J. Neural Eng.* **2019**, *16*, 011001.

[29] S. K. Ameri, M. Kim, I. A. Kuang, W. K. Perera, M. Alshiekh, H. Jeong, U. Topcu, D. Akinwande, N. Lu, *NPJ 2D Mater. Appl.* **2018**, *2*, 19.

[30] S. Mishra, Y. Lee, D. S. Lee, W. Yeo, presented at 2017 IEEE 67th Electron. Compon. Technol. Conf. (ECTC), 30 May–2 June **2017**.

[31] S. Mishra, J. J. S. Norton, Y. Lee, D. S. Lee, N. Agee, Y. Chen, Y. Chun, W.-H. Yeo, *Biosens. Bioelectron.* **2017**, *91*, 796.

[32] X. Pu, H. Guo, J. Chen, X. Wang, Y. Xi, C. Hu, Z. L. Wang, *Sci. Adv.* **2017**, *3*, e1700694.

[33] S. R. Soekadar, M. Witkowski, C. Gómez, E. Opisso, J. Medina, M. Cortese, M. Cempini, M. C. Carrozza, L. G. Cohen, N. Birbaumer, N. Vitiello, *Sci. Rob.* **2016**, *1*, eaag3296.

[34] J. Heo, H. Yoon, S. K. Park, *Sensors* **2017**, *17*, 1485.